Magnetic ordering and crystal field effects in the $R_2Ir_3Sn_5$ (R = La–Nd, Gd–Tm) system

N. S. Sangeetha,[1,*] A. Thamizhavel,[2] C. V. Tomy,[3] Saurabh Basu,[1] S. Ramakrishnan,[2] and D. Pal[1]

[1]*Department of Physics, Indian Institute of Technology Guwahati, Guwahati, Assam-781039, India*

[2]*Department of Condensed Matter Physics and Materials Science, Tata Institute of Fundamental Research, Homi Bhabha Road, Colaba, Mumbai-400005, India*

[3]*Department of Physics, Indian Institute of Technology Bombay, Mumbai-400076, India*

(Received 30 May 2011; published 26 August 2011)

We report on the detailed magnetic properties of polycrystalline ternary rare-earth intermetallic stannide compounds $R_2Ir_3Sn_5$ (R = La–Nd, Gd–Tm). Except for $La_2Ir_3Sn_5$, all the other compounds of $R_2Ir_3Sn_5$ (R = Ce–Nd, Gd–Tm) crystallize in the orthorhombic $Y_2Rh_3Sn_5$($Cmc2_1$) type structure. $La_2Ir_3Sn_5$ crystallizes in the $U_2Co_3Si_5$ type orthorhombic crystal structure with the space group *Ibam*. Transport and magnetization measurements were done from 1.8 to 300 K and the heat-capacity measurement was done from 2 to 30 K. We found from the magnetic measurements that $Ce_2Ir_3Sn_5$ is a Kondo system, which undergoes an antiferromagnetic ordering at 2.9 K, while no magnetic ordering was observed in $Pr_2Ir_3Sn_5$ and $Nd_2Ir_3Sn_5$ down to 1.8 K. The higher rare earths from Gd–Tm of this series exhibit magnetic ordering below 10 K. Crystal field analysis was done on both the magnetic susceptibility and heat capacity to find the crystal field level schemes. From the detailed magnetic measurements, we found that the magnetic ordering temperature deviates from the expected de Gennes scaling, which indicates that the RKKY interaction needs to be modified, including the crystal field effects, to account for this deviation.

DOI: 10.1103/PhysRevB.84.064430 PACS number(s): 81.10.−h, 71.27.+a, 71.70.Ch, 75.10.Dg

I. INTRODUCTION

Rare-earth ternary intermetallic compounds of the type $R_2T_3X_5$, where T is a transition metal and X is the s-p metal, have been widely investigated owing to their interesting magnetic properties.[1–3] These properties are related to the interaction between the localized f electrons from rare-earth elements and the itinerant conduction electrons of the surrounding atoms. The interesting ground states include superconductivity, the coexistence of magnetism and superconductivity, along with valence fluctuation, Kondo behavior, large positive magnetoresistance, and charge and spin density waves (CDW and SDW). In the early 1980s, considerable investigations were carried out to understand the superconductivity and magnetism in the $R_2Fe_3Si_5$ system.[4–6] In this family, Fe atoms do not carry any magnetic moment, but help in building large density of states at the Fermi level. $Tm_2Fe_3Si_5$ is a reentrant superconductor where superconductivity is destroyed by purely antiferromagnetic order.[7] It is worthwhile to point out that the compound $Lu_2Fe_3Si_5$ shows disorder-sensitive superconductivity below 6.2 K.[8] $Er_2Fe_3Si_5$ shows superconductivity below incommensurate and commensurate antiferromagnetic transitions.[9] The stannides compounds of $Ce_2Rh_3Sn_5$ (Ref. 10) and $Yb_2Pt_3Sn_5$ (Ref. 11) are both moderate heavy-fermion compounds, with mixed-valence behavior in the latter. Among the germanides family, $Ce_2Ir_3Ge_5$ is a Kondo lattice system with antiferromagnetic ordering and moderate heavy-fermion behavior.[12] $Pr_2Rh_3Ge_5$ have revealed heavy-fermion behavior due to crystal field excitations.[13] Recently, Yogesh *et al.* have reported the coexistence of superconductivity and charge density wave in $Lu_2Ir_3Si_5$.[14] It has also been revealed that there is a coexistence of charge density waves with normal regions.[15] As a result, it is noticed that a large number of compounds having $R_2T_3X_5$ formula with similar crystal structure have a variety of ground states. But, until today, comprehensive studies of R_2(Ir,Rh,Ni)$_3$(Si,Ge,Sn)$_5$ is not pursued. It is worthwhile to mention that compounds of silicides exist in tetragonal ($P4/mnc$, No. 140) structure while the other 2-3-5 members such as rhodium silicides, rhodium stannides, iridium germanides, and platinum indides form in orthorhombic structure, albeit with different space groups, namely, *Ibam, Cmc2*$_1$, *Pmmn,* and *Pnma,* respectively.[16–19] Here, we report the magnetic properties of $R_2Ir_3Sn_5$ series. Since Ir and Sn atoms do not carry any magnetic moment, the magnetic properties of these compounds are governed by conduction-electron mediated exchange interactions on the rare-earth moments, and by the effect of crystalline electric field (CEF) acting on the 4f electrons. Hence, it will be of interest to study magnetism and influence of CEF on magnetic ordering in the $R_2Ir_3Sn_5$ family. With this in view, as a part of our detailed study on this series, we report the transport, magnetic, and thermal properties observed from systematic studies carried out for $R_2Ir_3Sn_5$ (R = La, Ce–Nd, Gd–Tm) compounds.

II. EXPERIMENT

The polycrystalline samples of $R_2Ir_3Sn_5$ (R = La, Ce–Nd, Gd–Tm) were prepared by the usual arc melting method. The stoichiometric proportions of each constituent element were taken separately and then melted together by using arc furnace on a water-cooled copper hearth under Ti gettered in an atmosphere of continuously flowing argon gas. The purity of rare-earth metals was 99.9%, whereas the purity of Ir and Sn were 99.999%. The resulting alloy buttons were turned over and remelted several times to promote homogeneity. The as-cast compounds were wrapped in the tantalum foil, sealed in a quartz tube under vacuum, and annealed at 900 °C for 8 days. The small pieces of annealed $R_2Ir_3Sn_5$ (R = La, Ce–Nd, Gd–Tm) samples were used for room-temperature powder x-ray diffraction (XRD) with Cu Kα radiation by using PANalytical commercial x-ray diffractometer. The XRD

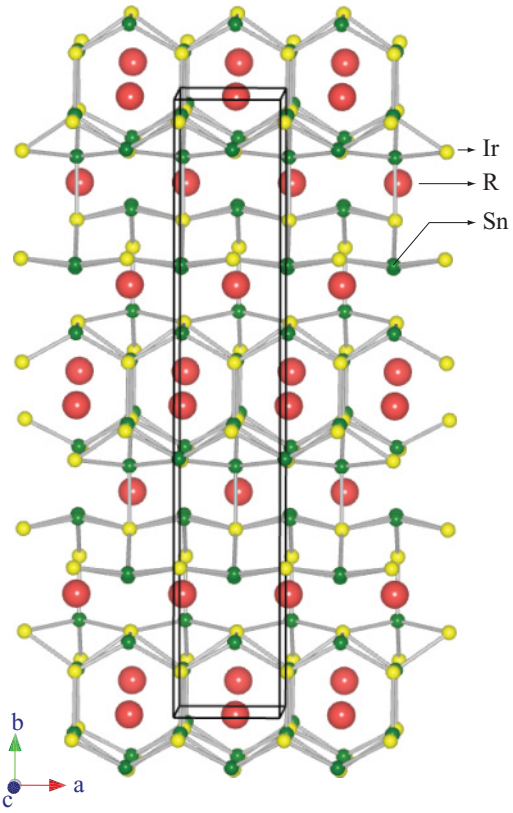

FIG. 1. (Color online) Crystal structure of the unit cell of the series $R_2Ir_3Sn_5$ (R: medium isolated red spheres, Ir : small yellow spheres, and Sn: small green spheres).

pattern of the samples confirmed the structure and the absence of any impurity phases. The compounds $R_2Ir_3Sn_5$ with R = Ce–Nd, Gd–Tm were found to adopt the orthorhombic ($Cmc2_1$) $Y_2Rh_3Sn_5$ (Ref. 20) structure; however, $La_2Ir_3Sn_5$, crystallizes in an orthorhombic $U_2Co_3Si_5$ (*Ibam*) type structure. The initial structural model for $R_2Ir_3Sn_5$ was generated from the atomic positions reported for isostructural and parent compound $Y_2Rh_3Sn_5$ by Meot-Meyer *et al.* and, later, it was used in subsequent refinement procedure. The lattice constants a, b, and $c$in series$R_2Ir_3Sn_5$ were estimated from Reitveld fit to their x-ray diffraction patterns using the FULLPROF program.[21] The lattice parameters obtained from this analysis are listed in Table I, where we notice that lattice volume decreases from lighter to heavier rare-earth elements. The unit cell of orthorhombic $R_2Ir_3Sn_5(Cmc2_1)$ structure is shown in Fig. 1. It is evident from Fig. 1 that $R_2Ir_3Sn_5$ possesses three-dimensional structure, being built up of two-dimensional Ir-Sn rings, which, when stacked in the a direction, encapsulated R atoms in three-dimensional channels. In $R_2Ir_3Sn_5$, R atoms reside in distorted pentagonal ([100] direction) and hexagonal ([001] direction) channels created by the Ir and Sn atoms. The local coordination environments for the Ir atoms can be described as distorted monocapped trigonal prisms. The Ir-Sn and Sn-Sn distances are considerably longer than the sum of the covalent radii of Ir and Sn. The unit cell for $La_2Ir_3Sn_5$ has a single La site, two Ir sites, and three Sn sites, whereas $R_2Ir_3Sn_5$ forms noncentrosymmetric ($Cmc2_1$) structure, which results in two R sites, three Ir sites, and five Sn sites, all on 4a Wyckoff positions. Hence, the hybridization between d and f orbitals is different for these two crystal structures, and it has to be taken into account in further analysis of magnetization measurements.

TABLE I. Lattice parameters of $RE_2Ir_3Sn_5$.

Sample	a (Å)	b (Å)	c (Å)	v (Å^3)
$La_2Ir_3Sn_5$[a]	10.781	12.958	6.327	884.356
$Ce_2Ir_3Sn_5$	4.471	26.443	7.261	858.499
$Pr_2Ir_3Sn_5$	4.468	26.474	7.254	858.045
$Nd_2Ir_3Sn_5$	4.457	26.444	7.246	854.021
$Gd_2Ir_3Sn_5$	4.408	26.304	7.211	836.101
$Tb_2Ir_3Sn_5$	4.400	26.241	7.200	831.314
$Dy_2Ir_3Sn_5$	4.395	26.256	7.195	830.267
$Ho_2Ir_3Sn_5$	4.378	26.346	7.185	828.737
$Er_2Ir_3Sn_5$	4.370	26.277	4.178	824.253
$Tm_2Ir_3Sn_5$	4.366	26.295	7.173	823.488

[a]$U_2Co_3Si_5$ (Ibam) crystal structure.

The electrical resistivity in the temperature range from 1.8 to 300 K was measured using a home-built electrical resistivity set up with the standard dc four-probe technique. The temperature dependence of dc magnetic susceptibility (χ) was measured using a commercial superconducting quantum interference device (SQUID) magnetometer (MPMS5, Quantum Design, USA) in a field of 4 kOe for the temperatures between 1.8 to 300 K. The isothermal magnetization was measured in the fields up to 5 T. The heat-capacity measurement in zero field in the temperature range from 2 to 30 K was performed in a Quantum Design physical properties measurement system (PPMS).

III. RESULTS

A. Magnetic susceptibility and magnetization studies

1. *Magnetic susceptibility of $R_2Ir_3Sn_5$ (R = La, Ce–Tm)*

The temperature dependence of inverse dc susceptibility (χ^{-1}) of $R_2Ir_3Sn_5$ (R = Ce–Tm) measured in an applied field of 4 kOe is shown in Figs. 2 and 3. Insets show the low-temperature susceptibility χ behavior (and $d\chi/dT$ for $Gd_2Ir_3Sn_5$ and $Tb_2Ir_3Sn_5$) of the respective compounds.

The high-temperature ($100 < T < 300$ K) magnetization is fitted to the modified Curie-Weiss law, which is given by

$$\chi = \chi_0 + \frac{C}{T - \Theta_P}. \quad (1)$$

Here, χ_0 is the temperature-independent term including the diamagnetic susceptibility (χ_{dia}), which arises due to the presence of ion cores, the Pauli spin susceptibility (χ_{Pauli}) of the conduction electrons, and Landau susceptibility (χ_{Landau}) of the diamagnetic orbital contribution due to the conduction electrons. Θ_P is the Curie-Weiss temperature and C is the Curie constant, which can be written in terms of effective moments as

$$C(\text{emuK/mol}) = \frac{N_A(\mu_{eff})^2 x}{3\,k_B} \approx \frac{(\mu_{eff})^2 x}{8}, \quad (2)$$

where x is the number of magnetic rare-earth ions (R) per formula, N_A is the Avogadro number, and k_B is the Boltzmann constant. The Curie-Weiss fit is marked by a solid line in

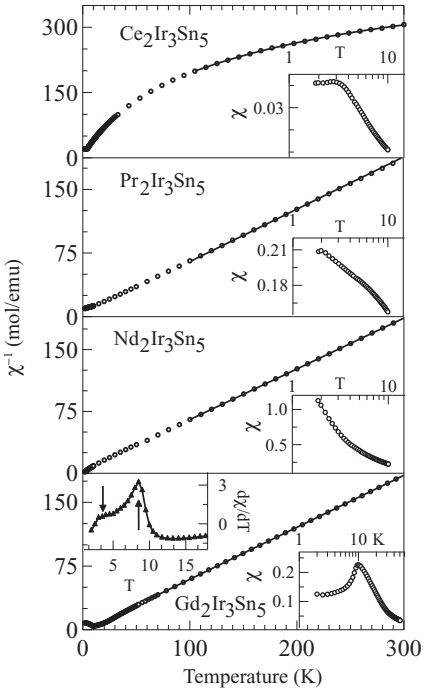

FIG. 2. Variation of inverse dc susceptibility (χ^{-1}) of $R_2Ir_3Sn_5$ (R = Ce–Gd) from 1.8 to 300 K in the field of 4 kOe. The inset shows the susceptibility (χ) behavior in low temperatures. The solid line is a fit to the Curie-Weiss relation.

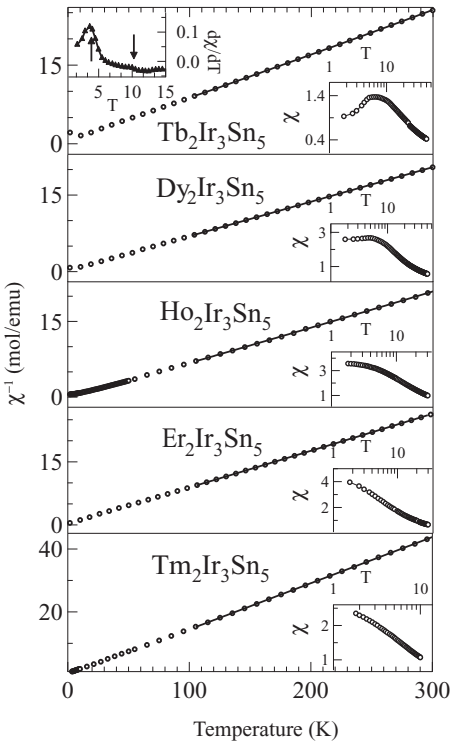

FIG. 3. Variation of inverse dc susceptibility (χ^{-1}) of $R_2Ir_3Sn_5$ (R = Tb–Tm) from 1.8 to 300 K in the field of 4 kOe. The inset shows the susceptibility (χ) behavior in low temperatures. The solid line is a fit to the Curie-Weiss relation.

the main plots of Figs. 2 and 3. The estimated effective moments, listed in Table II, for $R_2Ir_3Sn_5$ (R = Ce–Tm) samples are in good agreement with the Russel-Saunders values $\mu_{\text{eff}} = g\mu_B[J(J+1)]^{1/2}$, calculated for R^{3+} free ions, which indicate that the magnetic interaction of these compounds is mainly due to that of R^{3+} ions and there is no contribution from the Ir. But, in some compounds, the effective moment is found to be smaller than the moment of rare-earth (R^{3+}) free ions, which may be due to the presence of crystal field effects. Most of the compounds of lighter rare-earth elements show relatively small and negative values of the Curie-Weiss temperature (Θ_p), which implies the presence of antiferromagnetic correlations. The positive Θ_p indicates ferromagnetic correlation at high temperatures for heavier rare-earth-element-based compounds.

The low-temperature $\chi(T)$ data for most of the compounds, shown in the inset of Figs. 2 and 3, display small upturn in susceptibility, which possibly indicates the signature of the onset of antiferromagnetic ordering in these materials. The susceptibility of $Ce_2Ir_3Sn_5$ exhibits a cusp at 2.5 K corresponding to antiferromagnetic order. $Pr_2Ir_3Sn_5$ and $Nd_2Ir_3Sn_5$ do not reveal any magnetic ordering down to 1.8 K. The low-temperature $d(\chi)/dT$ versus T plot for $Gd_2Ir_3Sn_5$ and $Tb_2Ir_3Sn_5$ brings out multiple anomalies, which are marked by arrows. $Gd_2Ir_3Sn_5$ demonstrate two magnetic transitions at 3.2 and 9.5 K, while the magnetic ordering temperatures of $Tb_2Ir_3Sn_5$ are at 3.9 and 10 K. For $Dy_2Ir_3Sn_5$, the low-temperature χ data show single magnetic ordering (5 K) in contrast to multiple anomalies in heat capacity. $Ho_2Ir_3Sn_5$, $Er_2Ir_3Sn_5$, and $Tm_2Ir_3Sn_5$ exhibit antiferromagnetic orderings at 2, 1.9, and 1.9 K, respectively.

2. *M-H of $R_2Ir_3Sn_5$ (R = Ce, Pr, Gd, Tb, Dy, Ho, Er, and Tm)*

Figures 4 and 5 depict the magnetization measurements at various temperatures for $R_2Ir_3Sn_5$. In the case of $Ce_2Ir_3Sn_5$ at 3 and 2 K, the M-H behavior is linear until 5 T. The magnetization values of $Ce_2Ir_3Sn_5$ at high fields are quite small, presumably due to the presence of Kondo effect; the presence of Kondo effect is further supported by the resistivity data to be discussed in the next section. At higher temperatures (above transition temperature $T > T_N$), the usual linear behavior in M versus H is consistent with the paramagnetic state of the compound. The magnetization data for $Gd_2Ir_3Sn_5$ and $Tb_2Ir_3Sn_5$ depict *S-like* upward curvature, indicating the presence of metamagnetic transitions from a state of low

TABLE II. Magnetic data for $R_2Ir_3Sn_5$ compounds obtained from the high-temperature susceptibility fit to Curie-Weiss relation. μ_{th} is the theoretical free ion value for trivalent rare-earth ions.

Sample	χ_0 (emu/mol K)	μ_{eff} (μ_B)	μ_{th} (μ_B)	Θ_p (K)
$Ce_2Ir_3Sn_5$	2.1×10^{-3}	2.57	2.54	−37.5
$Pr_2Ir_3Sn_5$	8.56×10^{-6}	3.60	3.62	−5.28
$Nd_2Ir_3Sn_5$	1.01×10^{-4}	3.58	3.58	−5.65
$Gd_2Ir_3Sn_5$	1.14×10^{-6}	7.23	7.94	2.99
$Tb_2Ir_3Sn_5$	6.5×10^{-4}	9.75	9.7	−5.77
$Dy_2Ir_3Sn_5$	5.8×10^{-4}	10.8	10.65	−1.78
$Ho_2Ir_3Sn_5$	1.2×10^{-4}	10.56	10.61	7.33
$Er_2Ir_3Sn_5$	5.1×10^{-4}	9.43	9.59	1.80
$Tm_2Ir_3Sn_5$	9.5×10^{-4}	7.14	7.56	9.01

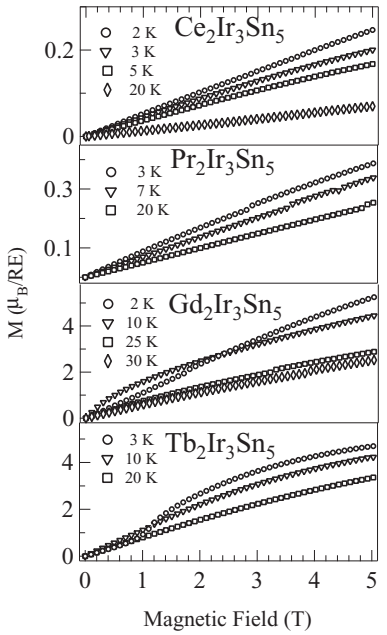

FIG. 4. Isothermal magnetization measurement of field dependence in $R_2Ir_3Sn_5$ series of compounds with R = Ce, Pr, Gd, and Tb.

magnetization to one of relatively high magnetization. Similar behavior has already been reported in some other Gd- and Tb-based compounds of the related crystal structure.[12,22] The magnetization of $Dy_2Ir_3Sn_5$ at 2 and 7 K exhibits nonlinear behavior, which suggests that similar magnetic correlation occurs in-between these temperature regions. The rest of the heavier rare-earth-based compounds exhibit nonlinear behavior at low temperatures, suggesting antiferromagnetic correlations in this temperature region. The magnetic moment of $Ho_2Ir_3Sn_5$ sort to saturate, reaching a value of about

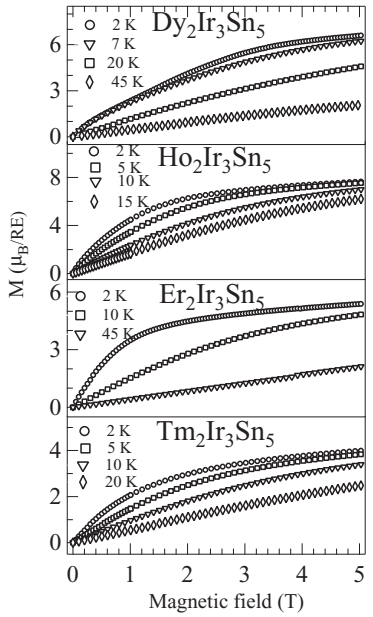

FIG. 5. Isothermal magnetization measurement of field dependence in $R_2Ir_3Sn_5$ series of compounds with R = Dy, Ho, Er, and Tm.

7.7 μ_B/R at 5 T, which is much lower than the value of 10.0 μ_B/R for Ho^{3+} saturated moment, at large applied field, which indicates the possibility for a metamagnetic transition at high fields. The similar effect is noticed in $Er_2Ir_3Sn_5$ and $Tm_2Ir_3Sn_5$. The nonlinearity in M versus H above T_N in the case of Dy, Ho, Er, and Tm indicates the possibility for short-range magnetic correlation [could arise due to splitting of energy levels by crystalline electric field (CEF)] still persists above Néel temperature. More investigation such as neutron-scattering (elastic and inelastic) measurements are essential to solve the magnetic structures and CEF levels of these compounds.

B. Resistivity studies of $R_2Ir_3Sn_5$ (R = La, Ce–Tm)

The electrical resistivity (ρ) data as a function of temperature in the range 1.8 to 300 K of $R_2Ir_3Sn_5$ (R = La, Ce–Tm) are presented in Figs. 6 and 7. The inset shows low temperature ρ (ρ_{mag} for $Ce_2Ir_3Sn_5$) versus T plot of respective compound on an expanded scale. The magnetic contribution is obtained by subtracting the resistivity of $La_2Ir_3Sn_5$ from that of $Ce_2Ir_3Sn_5$. The large value of the residual resistivity is due to the microcracks present in the sample. Since the properties of the 2-3-5 stannides are highly anisotropic, single crystals of these samples await for complete analysis. The resistivity of $La_2Ir_3Sn_5$ depicts an usual metallic behavior down to 1.8 K in contrast to the other germanides and silicides

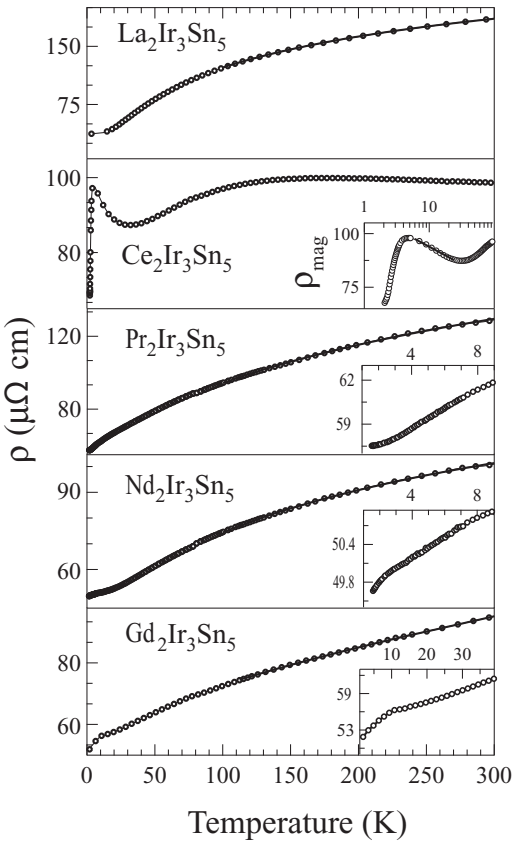

FIG. 6. The temperature dependence of resistivity (ρ) of $R_2Ir_3Sn_5$ (R = La–Nd and Gd) from 1.8 to 300 K. The inset shows low-temperature ρ data. The solid line in the main plots are fit to parallel resistor model.

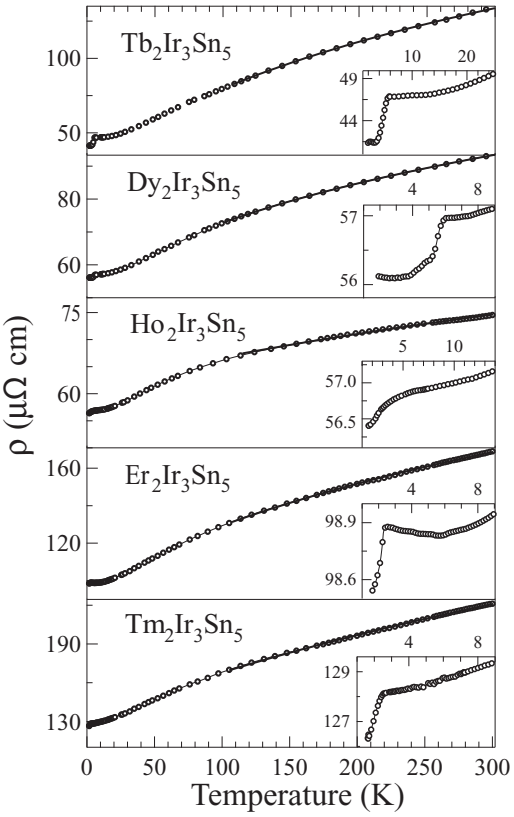

FIG. 7. The temperature dependence of resistivity (ρ) of $R_2Ir_3Sn_5$ (R = Tb–Tm) from 1.8 to 300 K. The inset shows low-temperature ρ data. The solid line in the main plots are fit to parallel resistor model.

and other 2-3-5 series.[10,12,16] The resistivity of $Ce_2Ir_3Sn_5$ displays a typical Kondo-type response with a minimum (ρ_{min}) around 30 K followed by a maximum of $\rho(T)$ at 4 K, indicating the onset of coherence. Subsequently, the resistivity falls sharply below 3 K, which clearly exhibits reduction in spin-disorder scattering caused by the antiferromagnetic ordering of the magnetic moments as seen in susceptibility data. The solid line shown in ρ_{mag} $Ce_2Ir_3Sn_5$ (inset of Fig. 6) is a fit to the relation $\rho_{mag}(T) = \rho_s - C_k \ln(T/T_k)$. This $-\ln T$ behavior in resistivity data suggests that this is a Kondo system. $Pr_2Ir_3Sn_5$ and $Nd_2Ir_3Sn_5$ do not show any signature of magnetic ordering down to 1.8 K, which corroborates the magnetization measurements. The low-temperature resistivity data for $Gd_2Ir_3Sn_5$ and $Tb_2Ir_3Sn_5$ reveal the magnetic ordering depicted by a slope change at 5.2 and 4.7 K, respectively. The plot of the derivative $d\rho/dT$ versus T (not presented here) brings out second anomalies around 10 and 9.7 K, respectively, on these compounds as observed in susceptibility data. The changes of the resistivity with temperature for rest of the rare-earth compounds (insets in Figs. 6 and 7) manifest clearly the magnetic ordering, which matches with susceptibility measurements. The transition temperatures obtained from resistivity measurement are listed in Table III along with those values obtained from susceptibility and heat-capacity studies.

TABLE III. Transition temperatures T_N observed from different measurement techniques.

Sample	Resistivity T_N (K)	Susceptibility T_N (K)	Heat capacity T_N (K)
$Ce_2Ir_3Sn_5$	2.5	2.42	2.9
$Pr_2Ir_3Sn_5$	-	-	-
$Nd_2Ir_3Sn_5$	-	-	-
$Gd_2Ir_3Sn_5$	5, 9.2	3, 9	3.34,9.2
$Tb_2Ir_3Sn_5$	4.7, 9.73	3.85, 10	4.9,10.11
$Dy_2Ir_3Sn_5$	5.31	5	4.38,5.23
$Ho_2Ir_3Sn_5$	2.48	2	< 2.5
$Er_2Ir_3Sn_5$	2.2	1.9	< 2.5
$Tm_2Ir_3Sn_5$	1.91	1.9	< 2.5

In the paramagnetic state, i.e., above magnetic transition temperatures ($T_N < T < 20$ K), the $\rho(T)$ is fitted to power law, which can be written as

$$\rho = \rho_0 + aT^n. \quad (3)$$

The values of ρ_0, a, and n are given in Table IV. We obtain a value of $n = 3$ for $La_2Ir_3Sn_5$. This value of n agrees with Wilson's *s-d* scattering model, which predicts a T^3 dependence of resistivity for transition-metal alloys below $\theta_D/10$, where θ_D is the Debye temperature. Since the compound $Ce_2Ir_3Sn_5$ exhibits Kondo effect, we have not made any attempt for power-law fit on $Ce_2Ir_3Sn_5$. The resistivity of the magnetic rare-earth compounds with R = Nd, Dy, Ho, and Er show a T^2 dependence in power-law fit. For $Tb_2Ir_3Sn_5$, it exhibits $T^{2.5}$ dependence. However, ρ of both $Gd_2Ir_3Sn_5$ and $Tm_2Ir_3Sn_5$ as well as $Pr_2Ir_3Sn_5$ show a different power-law dependence such as $T^{1.5}$ and T, respectively. At present, we do not understand the reason for this different power-law behavior.

At high temperatures (100 K $< T <$ 300 K), the resistivity data deviate significantly from the expected linear temperature dependence. Such a deviation from linear temperature dependence has been seen in many alloys and, subsequently, it shows a tendency to saturate where the value of ρ becomes sufficiently large. When the mean-free path is of the order of a few atomic spacing, the scattering cross section will no longer be linear in the scattering perturbation. Since the dominant temperature-dependent scattering mechanism here is electron-phonon interaction, the ρ will no longer be

TABLE IV. Parameters obtained from power-law fit in low-temperature resistivity for $R_2Ir_3Sn_5$.

Sample	ρ_0 ($\mu\Omega$ cm)	a (nΩ cm/K^n)	n (n)
$La_2Ir_3Sn_5$	37.05	1.05	3
$Pr_2Ir_3Sn_5$	50.87	20.7	1
$Nd_2Ir_3Sn_5$	50.54	5.01	2
$Gd_2Ir_3Sn_5$	55.32	25.01	1.5
$Tb_2Ir_3Sn_5$	46.58	1.03	2.5
$Dy_2Ir_3Sn_5$	56.76	3.02	2
$Ho_2Ir_3Sn_5$	56.74	2	2
$Er_2Ir_3Sn_5$	97.89	21	2
$Tm_2Ir_3Sn_5$	128	40	1.5

proportional to the mean-square atomic displacement, which is proportional to T for a harmonic potential. Instead, the resistance will rise less rapidly than T and will show a negative curvature ($d^2\rho/dT^2 < 0$). This behavior was also seen in previous studies on silicides and germanides.[23,24]

The high temperature $\rho(T)$ of these compounds would be treated by the well-described model, namely, as the parallel resistor model.[25] In this model, the expression of $\rho(T)$ is given by

$$\frac{1}{\rho(T)} = \frac{1}{\rho_1(T)} + \frac{1}{\rho_{\max}}, \tag{4}$$

where $\rho_{\max}$ is a saturation resistivity, which is independent of temperature, and $\rho_1(T)$ is the ideal temperature-dependent resistivity, which can be given by the expression

$$\rho_1(T) = \rho_0 + C_1\left(\frac{T}{\theta_D}\right)^5 \int_0^{\theta_D/T} \frac{x^5 dx}{[1-\exp(-x)][\exp(x)-1]}, \tag{5}$$

where ρ_0 is the residual resistivity and the second term is due to phonon-assisted electron scattering similar to the s-d scattering in transition-metal alloys. $x = h\omega_D/2\pi k_B T, \theta_D$ is the Debye temperature and C_1 is a numerical constant, which describes a temperature-independent interaction strength of the conduction electrons with the thermally excited phonons and contains the ionic mass, Fermi velocity, etc. Equation (4) can be derived if we assume that the electron mean-free path l is replaced by $l + a$ (a being average interatomic spacing). Such an assumption is reasonable since infinitely strong scattering can only reduce the electron mean-free path to a. Within the framework of Boltzmann transport equation, Chakraborty and Allen investigated the consequences of strong electron-phonon interaction. They found that *"nonclassical channels"* open up due to interband scattering, which accounts for the parallel resistor model.[26] The various parameters obtained by fitting the parallel resistor model to the high-temperature (100 K $< T <$ 300 K) ρ data of $R_2Ir_3Sn_5$ are listed in Table V and compared with the θ_D values estimated from heat-capacity data.

C. Heat-capacity studies of $R_2Ir_3Sn_5$ (R = La–Tm)

The temperature dependence of the the heat capacity (C_P) and magnetic entropy ($S_{\rm mag}$) from 1.8 to 30 K for $R_2Ir_3Sn_5$ (R = La–Tm) are shown in Figs. 8 and 9. The inset shows $C_{\rm mag}/T$ (C_P/T for $La_2Ir_3Sn_5$) versus T^2 at low temperature to illustrate the onset of bulk magnetic ordering in these samples.

TABLE V. $R_2Ir_3Sn_5$ series at high temperature (100 $< T <$ 300 K) using parallel resistor model. θ_D(HC) is observed from heat-capacity studies.

Sample	$\rho_{\max}$ ($\mu\Omega$ cm)	ρ_0 ($\mu\Omega$ cm)	C_1 ($\mu\Omega$ cm)	θ_D(fit) (K)	θ_D(HC) (K)
$La_2Ir_3Sn_5$	278	81	1097	180	188
$Pr_2Ir_3Sn_5$	214	106	573	191	189
$Nd_2Ir_3Sn_5$	156	86	554	200	205
$Gd_2Ir_3Sn_5$	236	88	256	260	254
$Tb_2Ir_3Sn_5$	303	60	523	213	217
$Dy_2Ir_3Sn_5$	160	103	144	247	242
$Ho_2Ir_3Sn_5$	137	120	170	274	237
$Er_2Ir_3Sn_5$	318	163	505	190	188
$Tm_2Ir_3Sn_5$	518	198	581	227	215

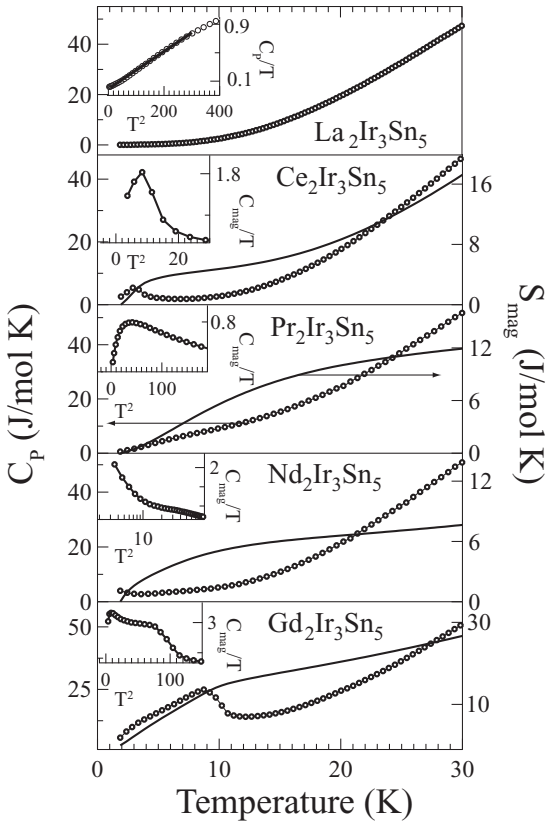

FIG. 8. Temperature dependence of the heat capacity [(C_P), marked by ($-\bigcirc-$)] of $R_2Ir_3Sn_5$ (R = La–Nd and Gd) from 1.8 to 30 K. The calculated entropy $S_{\rm mag}$ (solid line) (after subtractions of lattice contribution from C_P of $La_2Ir_3Sn_5$) is shown in the right-hand side of the same figure. The inset shows the low-temperature $C_{\rm mag}/T$ vs T^2 data.

The temperature dependence of heat capacity (C_P) for $R_2Ir_3Sn_5$ (R = Ce–Tm) is fitted to the expression

$$C_{\rm tot} = C_{\rm elec} + C_{\rm ph} = \gamma T + \beta T^3, \tag{6}$$

where γ is due to the electronic contribution and β is due to the phononic contribution. From the β value, we can estimate the value of Debye temperature θ_D by using the relation

$$\theta_D = \left(\frac{12\pi^4 N r k_B}{5\beta}\right)^{1/3}, \tag{7}$$

where N is the Avogadro's number, r is the number of atoms per formula unit, and k_B is the Boltzmann's constant. The value of θ_D calculated from C_P data is included in Table V to alleviate the comparison with Debye temperatures from high-temperature resistivity data. The parameters obtained from the analysis of heat-capacity measurements can be found in Table VI, where we have listed values of the ordering temperature T_N, entropy $S_{\rm mag}(T_N)/R$, $S_{\rm mag}(30\ K)/R$ for different members of the $R_2Ir_3Sn_5$ series, along with expected value of entropy of trivalent rare-earth ion $R\ln(2J+1)$.

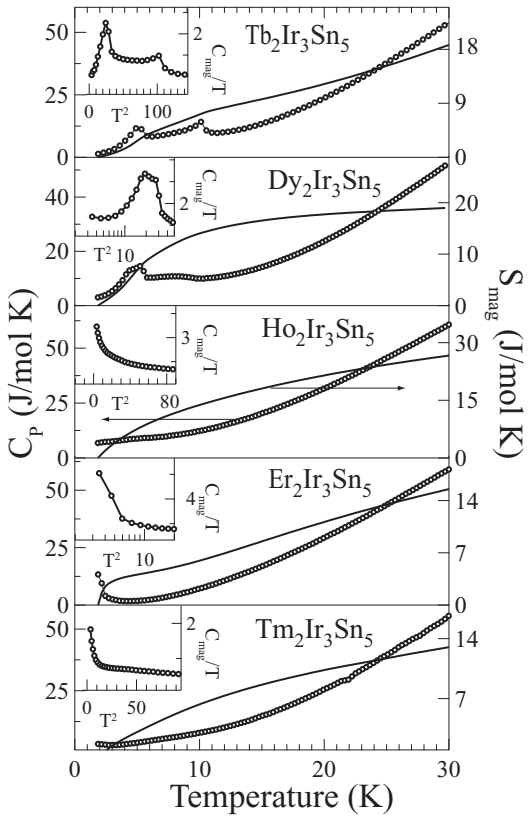

FIG. 9. Temperature dependence of the heat capacity [(C_P),markedby$(-\bigcirc-)$] of $R_2Ir_3Sn_5$ (R = Dy–Tm) from 1.8 to 30 K. The calculated entropy S_{mag} (solid line) (after subtraction of lattice contribution from C_P of $La_2Ir_3Sn_5$) is shown in the right-hand side of the same figure. The inset shows the low-temperature C_{mag}/T vs T^2 data.

The fit to C_P/T versus T^2 for the $La_2Ir_3Sn_5$ sample (see the inset) estimates the value of Sommerfeld's coefficient γ as 9.4 mJ/mol K^2, which agrees closely with that observed for the free electrons of the mass of the La atom.[27] For $Ce_2Ir_3Sn_5$, the large peak in C_{mag}/T at 2.9 K confirms the bulk magnetic ordering of Ce^{3+} moments. The fit to heat-capacity data using Eq. (6) in the temperature range from 10 to 20 K yielded the value of γ as 58 mJ/mol K, which suggests that the $Ce_2Ir_3Sn_5$ is a moderate heavy-fermion antiferromagnet.

The temperature dependence of C_P for $Pr_2Ir_3Sn_5$ and $Nd_2Ir_3Sn_5$ reveals no bulk magnetic ordering down to 1.8 K, in these samples. The C_{mag}, derived by subtracting the lattice contribution from C_P, show a broad hump in $Pr_2Ir_3Sn_5$ and $Nd_2Ir_3Sn_5$ around 8 and 10 K, respectively, which demonstrates Schottky-type anomaly indicating the presence of low-lying excited crystal electric field (CEF) level becoming populated with the increase of temperature. The low value of estimated entropy at 30 K as well as the large value of Sommerfeld coefficients may be accounted for either by the CEF effects or by short-range magnetic correlations. The C_{mag} of $Gd_2Ir_3Sn_5$ displays transitions at 4.32 and 10.21 K, indicating bulk magnetic ordering of Gd^{3+} spins, which is in agreement with the susceptibility and resistivity data. It is conjectured that a second anomaly at 4.32 K may be associated with the moment reorientation effect as noticed in other intermetallic compounds.[10,28,29] The entropy at 30 K is found to be 3.19 R, which is more than the expected value of $R\ \ln(2J+1)$. The large value of entropy may be due to the short-range correlation above the magnetic ordering.

The C_{mag} data of $Tb_2Ir_3Sn_5$ and $Dy_2Ir_3Sn_5$ reveal two bulk magnetic transitions. The transition for $Tb_2Ir_3Sn_5$ occurs at 4.9 and 10.2 K, which upholds results from the susceptibility and resistivity data. The entropy at 30 K is nearly equal to the expected value of the free ion. For $Dy_2Ir_3Sn_5$, the main transition at 5.23 K is consistent with resistivity and susceptibility measurements. The second anomaly at 4.38 K is observed only in heat-capacity data, which may originate due to successive spin reorientation effects. The Schottky anomaly is depicted by a broad hump around 15 K.

The heat-capacity data for $Ho_2Ir_3Sn_5$, $Er_2Ir_3Sn_5$, and $Tm_2Ir_3Sn_5$ show an upturn at low temperature below 4 K, which continues down to the lowest measured temperature, and this confirms the onset magnetic ordering of R^{3+} moments, which was seen in susceptibility and resistivity. Schottky-type anomaly suggests CEF effects in these compounds. All the heavier rare earths depict the low value of entropy at 30 K and very large γ, which indicates strong influence of hybridization in these compounds.

D. Crystal field analysis

We review the effect of the crystal fields on thermodynamic properties (heat capacity and magnetic susceptibility) of

TABLE VI. Parameters obtained from heat-capacity studies of $R_2Ir_3Sn_5$.

Sample	T_N (K)	$S_{mag}(T_N)/R$	J	$\ln(2J+1)$	$S_{mag}(30)/R$	B_2^0 (K)
$Ce_2Ir_3Sn_5$	2.9	0.35	$\frac{5}{2}$	1.79	1.89	-
$Pr_2Ir_3Sn_5$	-	-	4	2.19	1.43	3.2
$Nd_2Ir_3Sn_5$	-	-	$\frac{9}{2}$	2.3	0.92	1.9
$Gd_2Ir_3Sn_5$	3.34,9.2	1.6	$\frac{7}{2}$	2.08	3.19	-
$Tb_2Ir_3Sn_5$	4.9,10.11	1.4	6	2.57	2.13	-
$Dy_2Ir_3Sn_5$	4.38,5.23	0.9	$\frac{15}{2}$	2.77	2.3	1.2
$Ho_2Ir_3Sn_5$	< 2.5	1.09	8	2.83	3.2	2.7
$Er_2Ir_3Sn_5$	< 2.5	1.14	$\frac{15}{2}$	2.77	1.9	4.5
$Tm_2Ir_3Sn_5$	< 2.5	0.45	6	2.56	1.56	2.3

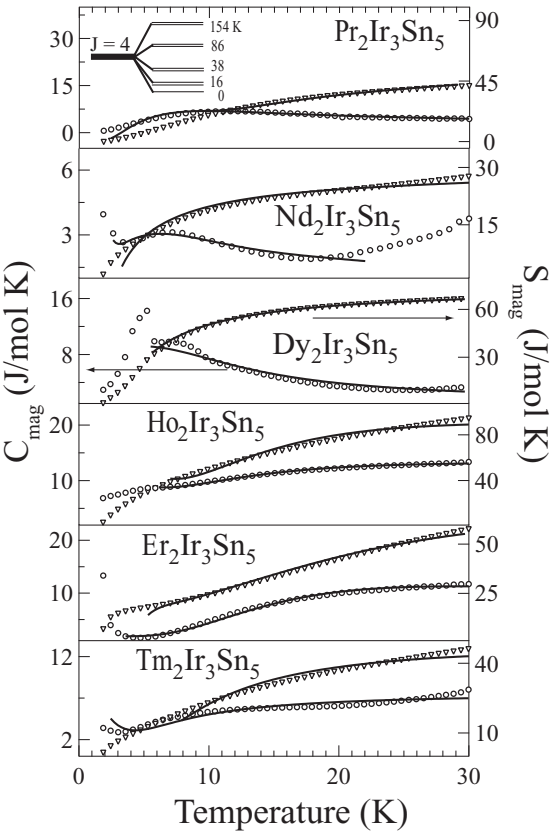

FIG. 10. Plot of the magnetic contribution to the heat capacity ($C_{\rm mag}$) and the entropy ($S_{\rm mag}$) vs T of $R_2Ir_3Sn_5$ (R = Pr, Nd, Dy, Ho, Er, and Tm). The solid lines are fit to the CEF model.

$R_2Ir_3Sn_5$ compounds, which has revealed signatures of CEF at low temperatures. Particularly in the case of the Ce system, the entropy and the magnetization are considerably low, which signals the CEF and Kondo effect. The magnetic contribution of heat capacity of $R_2Ir_3Sn_5$ is isolated by subtracting the heat capacity of the $La_2Ir_3Sn_5$, shown in Fig. 10. Hence, we provide an analysis of the magnetic interaction in terms of a combined crystal field and molecular field approach.

The Hamiltonian of a system for determining the magnetic properties of the material, consisting of spin-orbit coupling, crystalline electric field, Zeeman and exchange field terms, can be written as

$$\mathcal{H} = \lambda \overrightarrow{L} \cdot \overrightarrow{S} + \mathcal{H}_{\rm CEF} + \beta \overrightarrow{H} \cdot (\overrightarrow{L} + 2\overrightarrow{S}) + \mathcal{H}_{\rm ex}. \quad (8)$$

It is diagonalized within the substates arising from the lowest multiplets of R^{3+} (R = Pr, Nd, Dy, Ho, Er, and Tm) to obtain the energy and eigenfunctions of respective ions. In $R_2Ir_3Sn_5$ compounds, R^{3+} ions occupy two sites on 4*a* Wyckoff position in the orthorhombic $Y_2Rh_3Sn_5$- type structure, which belongs to the $Cmc2_1$ space group. In the orthorhombic symmetry of $R_2Ir_3Sn_5$, the effect of crystal structure on f electrons is characterized by seven real parameters, which include four cubic parameters. The limited experimental data prevented us from the independent determination of all the crystal field parameters unambiguously. In order to keep the number of parameters to a minimum, we retained the fourth-order cubic terms and second-order axial distortion term only. The CEF Hamiltonian for orthorhombic symmetry, after retaining only these terms, can be expressed as

$$\mathcal{H}_{\rm CEF} = B_2^0 O_2^0 + B_2^2 O_2^2, \quad (9)$$

where B_ℓ^m and O_ℓ^m are crystal field parameters (which measure the strength of crystal field) and the Steven's operators (in terms of angular momentum operators), respectively. B_2^0 and B_2^2 determine the strength of the crystal field due to axial and rhombic distortion. The diagonalization of the above Hamiltonian together with other detailed calculations can be done by using the standard procedure. By diagonalizing the CEF Hamiltonian, one can estimate consistent sets of energy eigenvalues and eigenvectors by which the explicit determination of heat capacity [using Eq. (10)] is possible. As revealed in other 2-3-5 compounds with similar crystal structure, the parameter B_2^2 is negligible compared to the B_2^0.[30] Hence, in our analysis, we have used B_2^0 as the only parameter to determine the strength of the crystalline electric field. The Schottky equation for the heat capacity in the presence of crystal field effects is given by

$$C_{\rm Sch} = \left[\frac{R\sum_i g e^{-E_i/T} \sum_i g_i E_i^2 e^{-E_i/T} \left(\sum_i g_i E_i e^{-E_i/T}\right)^2}{(k_B T)^2 \left(\sum_i g_i e^{-E_i/T}\right)^2} \right], \quad (10)$$

where R is a gas constant, E_i is the crystalline field energy levels in units of temperature, and g_i is the degeneracy of the energy levels. The estimation of CEF parameters is made by least-squares fitting of the experimental heat-capacity data using Eq. (10). The fit to the Schottky anomaly as well as to the total entropy of the magnetic heat capacities of $R_2Ir_3Sn_5$ (R = Pr, Nd, Dy, Ho, Er, and Tm) is displayed in Fig. 10. The crystal field split energy levels obtained from CEF parameters for one of the rare-earth samples $Pr_2Ir_3Sn_5$ is also shown in Fig 10. The summarized result from this analysis is listed in Table VII. In all the compounds, we found that the best fit was obtained for the positive crystal field parameter B_2^0.

The magnetic susceptibility of $R_2Ir_3Sn_5$ is analyzed on the basis of the CEF model including the exchange parameter. The exchange interaction, in the molecular field framework above the Néel temperature, is given by

$$\mathcal{H}_{\rm ex} = -2zJ \langle \overrightarrow{\mathbf{S}} \rangle \cdot \overrightarrow{\mathbf{S}}. \quad (11)$$

Here, z is the number of nearest equivalent neighbors interacting with the exchange interaction J, and $\langle \overrightarrow{\mathbf{S}} \rangle$ is the expectation

TABLE VII. Parameters obtained from CEF fit.

Sample	J	B_2^0	λ (mol/emu)	zJ
$Pr_2Ir_3Sn_5$	4	3.2	9.76	−0.3
$Nd_2Ir_3Sn_5$	$\frac{9}{2}$	1.9	3.1	−0.28
$Dy_2Ir_3Sn_5$	$\frac{15}{2}$	1.2	5	−2.7
$Ho_2Ir_3Sn_5$	8	2.7	3	−2.6
$Er_2Ir_3Sn_5$	$\frac{15}{2}$	4.5	4	−2.07
$Tm_2Ir_3Sn_5$	6	2.3	6.54	−1.24

value of the spin operator **S**. An iterative procedure were used to calculate $\langle \vec{\mathbf{S}} \rangle$ self-consistently. The details of this procedure were discussed by Marathe and Mitra.[31]

In order to show CEF effects on the susceptibility, we have used Van Vleck's susceptibility expression given by Cascales *et al.*[32] as follows:

$$\chi_{\mathrm{CEF}} = N\beta^2 \sum_a \left[\frac{\langle \phi_a | \mathcal{H} | \phi_a \rangle^2}{k_B T} - 2 \sum_b \frac{\langle \phi_a | \mathcal{H} | \phi_b \rangle \langle \phi_b | \mathcal{H} | \phi_a \rangle}{E_a - E_b} \right] \times \frac{\exp\left(-E_a^0 / k_B T\right)}{\sum_a \exp\left(-E_a^0 / k_B T\right)} \tag{12}$$

in which N is the Avogadro's number, β is the Bohr magneton, k_B is the Boltzmann constant, E and ϕ the nonperturbed eigenvalues and wave functions, respectively, described on the SLJM$_J$ basis. In a fitting procedure, the susceptibility has been taken as the average and corrected by a molecular field constant λ, i.e.,

$$\frac{1}{\chi_{\mathrm{exp}}} = \frac{1}{\chi_{\mathrm{CEF}}} - \lambda, \tag{13}$$

where $\lambda = Jz/(g_J \mu_B)^2$, which parametrizes the strength of the molecular field as a function of the magnetization. We have fixed the crystal field parameter B_2^0 obtained from an analysis of the heat-capacity data, and varied the exchange parameter $z\,J$ so as to obtain the best fit to the experimentally observed magnetic susceptibility data. The calculated magnetic susceptibility (χ_{CEF}) from Eq. (13) is in good agreement with the experimentally observed data of $R_2Ir_3Sn_5$ as shown in Fig. 11. The estimated value of $z\,J$ and molecular field constant λ for various $R_2Ir_3Sn_5$ compounds are listed in Table VII.

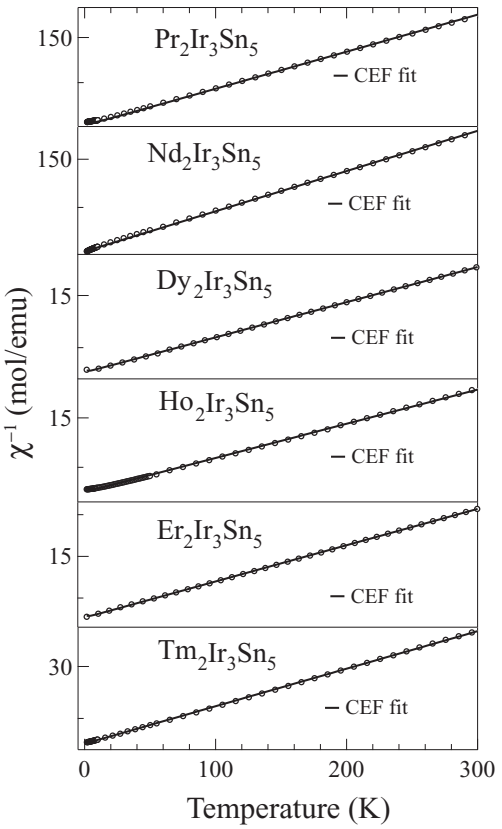

FIG. 11. Variation of the inverse susceptibility of $R_2Ir_3Sn_5$ (R = Pr, Nd, Dy, Ho, Er, and Tm) series in a field of 4 kOe from 2 to 300 K. The solid lines are fits to the CEF model.

IV. DISCUSSION

In this section, we make an attempt to understand the temperature dependence of the measured physical properties and the models that we have used to understand their behavior. We begin with the results derived from transport measurement. In magnetically ordered materials, the temperature-dependent part of the resistivity at low temperature is mainly due to electron-electron scattering, electron-phonon scattering, and electron-spin-wave scattering phenomena. In Table IV, we see T^2 dependence of certain compounds, which suggests that the spin fluctuation plays an important role in scattering conduction electrons at these temperatures. In the case of $Pr_2Ir_3Sn_5$, a linear temperature dependence is observed. This type of linear temperature dependence is also observed in other Pr-based compounds.[33] For $Tb_2Ir_3Sn_5$, we find a marked deviation from the T^2 law with n being equal to 2.5, and the reasons are not well understood at present. $Gd_2Ir_3Sn_5$ and $Tm_2Ir_3Sn_5$ exhibit $n = 1.5$ power-law dependence, which may be described in the framework of the spin-fluctuation theories of Moriya, Takimoto, and Lonzarich.[34,35] Based on this model, resistivity in the vicinity of three-dimensional antiferromagnetic transition scales as $T^{3/2}$ and scales as $T^{5/3}$ in the neighborhood of ferromagnetic transition.[36] It is important to mention that the effect of magnetic correlation in long-range order and disorder plays an important role in the spin-fluctuation model.

At higher temperatures above 100 K, the $\rho(T)$ dependence is not strictly linear, but has a small negative curvature. This deviation from the Bloch-Gruneisan law is attributed to the shape of the conduction-band density of d states and larger s-d type scattering. The high-temperature dependence of ρ is fitted to the parallel resistor model (see Table V), and the estimated value of θ_D agrees with those obtained from heat-capacity data for almost all compounds (magnetic or nonmagnetic) of the series $R_2Ir_3Sn_5$. The values of ρ_{max} vary considerably across the series and are quite high in most cases. The exact origin of the ρ_{max} is still not understood properly. In a recent semiclassical theory, the resistivity is related to the mean-free path λ by the relation $\rho = 3\pi h/e^2 k_F^2 \lambda$. The minimum mean-free path is taken as the interatomic distance based on the assumption that the electrons can be scattered at most by every atom. This leads to the saturation resistivity or the maximum resistivity ρ_{max} in this scheme. This value of ρ_{max} is called the Ioffe-Regel resistivity and, for most compounds, its value is about 150–200 $\mu\Omega$ cm. As noticed from Table V, that $\rho_0's$ for our samples is quite large, which is also seen in some recent systems with large resistivity, which saturate at values much larger values than the Loffe-Regel resistivity.[12] Thus, it is clear that both low- and high-temperature behaviors of the transport properties for $R_2Ir_3Sn_5$ compounds require more investigations for better understanding.

We now turn our attention to some of the systematic trends observed in magnetic properties at low and high temperatures.

The high-temperature susceptibility data for all the compounds are fitted to modified Curie-Weiss law. From Table II, it can be seen that the temperature-independent susceptibility χ_0 is non-negligible for some cases ($Ce_2Ir_3Sn_5$), which possibly indicates a large density of states at the Fermi level $N(E_F)$. Even in the presence of strong hybridization of $4f$ orbitals of Ce and the conduction electrons, which leads to Kondo effect in resistivity, we observe large values of θ_P (−37.5 K) in $Ce_2Ir_3Sn_5$, indicating the presence of antiferromagnetic correlations. For the rest of the compounds, the strength of the interactions between the R^{3+} ions is similar. We wish to recall here that the polycrystalline data are influenced by the overall behavior of the compound including the anisotropy.[37] The data begin to deviate from the Curie-Weiss behavior at lower temperatures, which was explained by CEF. The multiple anomalies in susceptibility and the deviation from linear behavior in magnetization curve below T_N for $Gd_2Ir_3Sn_5$ and $Tb_2Ir_3Sn_5$ can be attributed either to a change in the magnetic structure or to a manifestation of a small anisotropy via spin-flop phenomena.

We discuss the nature of the ground state of the energy level of the rare-earth ions in these materials on the basis of their magnetic entropy. In this discussion, where double magnetic transition is observed, we consider the value of entropy at the higher T_N as the difference between the $S_{mag}(T_{N1})$ and $S_{mag}(T_{N2})$ is about 1 J/mol K. The $S_{mag}(T_N)$ for $Ce_2Ir_3Sn_5$ reaches to the value of $0.35R$ ($\approx$ 50% ln 2)and then approaches $1.89R[\approx R\ln(2J+1)]$ at 30 K, which indicates that doublet ground states dominate the low-temperature properties of this compound, which ties in with the knowledge that Ce is a Krammer's ion. The value of entropy at 30 K for $Pr_2Ir_3Sn_5$ ($1.43R \approx R\ln 4$) and $Nd_2Ir_3Sn_5$ ($0.92R \approx R\ln 3$), which is much less than the expected value $R\ln(2J+1)$. $Pr_2Ir_3Sn_5$ exhibit singlet ground state arising from CEF splitting of $(2J+1)$ levels of non-Krammer's Pr^{3+} ion, whereas the Krammer's Nd^{3+} ions for $Nd_2Ir_3Sn_5$ exhibit doublet ground state, even though specific heat shows no signature of phase transition until the lowest available temperature. In the case of $Gd_2Ir_3Sn_5$, where no crystal field effects are present, S_{mag} at T_N ($1.6R \approx \ln 5$) is less than the expected total entropy $2.08R$ for the Gd^{3+} ion. But, the value of entropy gradually increases above T_N and, at 30 K, it is $3.19R$. The entropy for $Tb_2Ir_3Sn_5$ reaches a value of $1.4R$ ($\approx R\ln 4$)at T_N, which indicates that the ground state is a quartet for this compound. The full entropy is not released at 30 K in $Dy_2Ir_3Sn_5$, $Er_2Ir_3Sn_5$, and $Tm_2Ir_3Sn_5$ compounds, indicating that we need to go to further high temperatures to access all the higher energy levels created by the CEF. For $Ho_2Ir_3Sn_5$, the slightly higher value of entropy at 30 K from the expected $R\ln(2J+1)$ value suggests the possibility of inclusion of contribution to the magnetization from the transition element. From crystal field analysis, we found that the ground states of Dy and Er compounds are doublet, while $Tm_2Ir_3Sn_5$ and $Ho_2Ir_3Sn_5$ show singlet ground states.

We have determined magnetic ordering temperatures for $R_2Ir_3Sn_5$ using ρ, χ, and C_P measurements (see Table III). Both Gd and Tb show multiple transitions in all measurements, whereas the Dy compound exhibits multiple orderings only in heat-capacity data. For the purpose of analysis, we have considered transition temperatures obtained from the dc susceptibility measurements. In general, the antiferromagnetic ordering temperature T_N is given by[38]

$$T_N = \theta_P = \frac{3\pi n^2}{k_B E_F} J_{sf}^2 (g_J - 1)^2 J(J+1) \times \sum_{i \neq 0} F(2\,k_F R_{Oi}) \cos(k_o . R_{Oi}), \quad (14)$$

where E_F is the Fermi energy, J_{sf} is the exchange integral, k_o is the propagation vector of spins, R_{Oi} is the distance between the central ion O with its nearest neighbors i, and n is the density of conduction electrons. $F(x)$ is the Ruderman-Kittel-Kasuya-Yosida (RKKY) interaction, and is given by

$$F(x) = \frac{[\sin(x) - x\,\cos(x)]}{x^4}. \quad (15)$$

Normally, if CEF effects are not taken into account, the T_N of rare-earth members of the series are expected to follow the well-known de Gennes scaling[39] as $(g_J - 1)^2 J\,(J+1)$, where g_J is the Lande g factor and J is the total angular momentum of the local moment. If the angular momentum (L) is quenched, then T_N is expected to scale as $S(S+1)$.

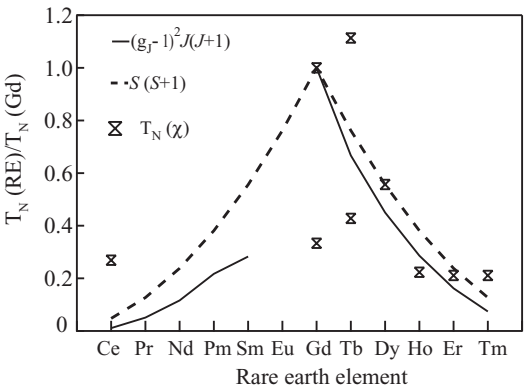

FIG. 12. Plots of the ordering temperature of the compounds of the series $R_2Ir_3Sn_5$ (R = Ce–Nd, Gd–Tm) normalized to the T_N value for Gd. The dashed lines are the theoretical de Gennes scaling with only spin quantum number and the solid lines are related to de Gennes scaling with total angular momentum.

Figure 12 depicts the comparison of T_N for those rare-earth compounds that undergo magnetic ordering (normalized to T_N value of Gd) with those expected on the basis of de Gennes scaling $(g_J - 1)^2 J\,(J+1)$ (solid line) as well as spin quantum number $S(S+1)$ (dashed line). It is evident that the ordering temperature of $Ce_2Ir_3Sn_5$ and $Tb_2Ir_3Sn_5$ are anomalously large compared to both de Gennes scaling $(g_J - 1)^2 J\,(J+1)$ and $S(S+1)$, while T_N's for the rest of the compounds follow the scaling curve of spin quantum number $S(S+1)$ better than de Gennes scaling $(g_J - 1)^2 J\,(J+1)$. It implies that the magnetic transitions occur not solely due to RKKY interaction. It is well known that the CEF (in the case of doublet ground state) can enhance the magnetic transition temperature, and this could, in principle, account for the difference between the observed data and de Gennes scaling.[40] However, it can also suppress the transition when singlet ground states are involved and the exchange interaction is weak. But, we believe that the reason for the discrepancy between observed T_N and that found from de Gennes scaling is not solely due to CEF.

V. CONCLUSION

In conclusion, we have synthesized rare-earth intermetallic compounds of the series $R_2Ir_3Sn_5$ with R = La, Ce–Nd, Gd–Tm. All the compounds containing magnetic rare-earth elements show antiferromagnetic ordering with the exception of $Pr_2Ir_3Sn_5$ and $Nd_2Ir_3Sn_5$, which do not show any transition down to 1.8 K. Among those, $Gd_2Ir_3Sn_5$, $Tb_2Ir_3Sn_5$, and $Dy_2Ir_3Sn_5$ exhibit multiple transitions. We have observed that the Curie-Weiss fit to $R_2Ir_3Sn_5$ gives an estimated effective moment μ_{eff} close to the free-ion R^{3+} values. The obtained values of θ_D from the parallel resistor model do agree well with those obtained from heat-capacity data. Most of the compounds belonging to $R_2Ir_3Sn_5$ series exhibit expected the T^2 power dependence of the resistivity data. A simple analysis of the crystal field model is proposed to account for the contribution to the magnetic entropy and susceptibility of magnetic rare-earth samples of this series.

ACKNOWLEDGMENTS

N. S. S. thanks H. R. Naren and R. P. Singh for the help in our experiment. C.V.T. would like to acknowledge the Department of Science and Technology for the partial support through the Project No. IR/S2/PV-10/2006.

*sangeetha@iitg.ac.in

[1]P. Rogl, in *Handbook of Physics and Chemistry of Rare Earths*, edited by K. A. Gschneidner, Jr., and L. Eyring (Elsevier, Amsterdam, 1984), Vol. 7, pp. 1–264.
[2]J. Leciejewicz and A. Szytula, in *Handbook of Physics and Chemistry of Rare Earths*, edited by K. A. Gschneidner, Jr., and L. Eyring (Elsevier, Amsterdam, 1989), Vol. 12, pp. 133.
[3]C. B. Vining and R. N. Shelton, Phys. Rev. B **28**, 2732 (1983).
[4]H. F. Braun, Phys. Lett. A **75**, 386 (1980).
[5]H. F. Braun, C. U. Segre, F. Acker, M. Rosenberg, S. Dey, and U. Deppe, J. Magn. Magn. Mater. **25**, 117 (1981).
[6]A. R. Moodenbaugh, D. E. Cox, and H. F. Braun, Phys. Rev. B **25**, 4702 (1982).
[7]J. A. Gotaas, J. W. Lynn, R. N. Shelton, P. Klavins, and H. F. Braun, Phys. Rev. B **36**, 7277 (1987).
[8]Tadataka Watanabe, Hiroki Sasame, Hiroaki Okuyama, Kouichi Takase, and Yoshiki Takano, Phys. Rev. B **80**, 100502(R) (2009)
[9]S. Noguchi and K. Okuda, Phys. B (Amsterdam) **194-196**, 1975 (1994)
[10]N. G. Patil and S. Ramakrishnan, Phys. Rev. B **59**, 12054 (1999).
[11]Y. Muro, Y. Yamane, M. S. Kim, T. Takabatake, C. Godart, and P. Rogl, J. Phys. Soc. Jpn. **72**, 1745 (2003)
[12]Yogesh Singh and S. Ramakrishnan, Phys. Rev. B **69**, 174423 (2004).
[13]V. K. Anand, Z. Hossain, and C. Geibel, Phys. Rev. B **77**, 184407 (2008).
[14]Yogesh Singh, Dilip Pal, S. Ramakrishnan, A. M. Awasthi, and S. K. Malik, Phys. Rev. B **71**, 045109 (2005).
[15]M. H. Lee, C. H. Chen, M. W. Chu, C. S. Lue, and Y. K. Kuo, Phys. Rev. B **83**, 155121 (2011)
[16]Yogesh Singh, D. Pal, and S. Ramakrishnan, Phys. Rev. B **70**, 064403 (2004).
[17]R. Pöttgen, A. Lang, R.-D. Hoffmann, B. Knnen, G. Kotzyba, R. Mllmann, B. D. Mosel, and C. Rosenhahn, Z. Kristallogr. **214**, 143 (1999).
[18]Y. V. Galadzhun, R. D. Hoffmann, R. Pöttgen, and M. Adam, J. Solid State Chem. **148**, 425 (1999).
[19]E. Parthe and B. Chabot, in *Handbook of Physics and Chemistry of Rare Earths*, edited by K. A. Gschneidner, Jr., and L. Eyring (Elsevier, Amsterdam, 1984), Vol. 7, pp. 113–333.
[20]M. Meot-Meyer, G. Venturini, B. Malaman, J. Seinmetz, and B. Roques, Mater. Res. Bull. **18**, 1181 (1984).
[21]Juan Rodriguez-Carvajal, Phys. B (Amsterdam) **55**, 192 (1993).
[22]N. G. Patil and S. Ramakrishnan, Phys. Rev. B **59**, 9581 (1999).
[23]S. Ramakrishnan, K. Ghosh, and Girish Chandra, Phys. Rev. B **45**, 10769 (1992).
[24]K. Ghosh, S. Ramakrishnan, and Girish Chandra, Phys. Rev. B **48**, 10440 (1993).
[25]H. Wiesmann, M. Gurvitch, H. Lutz, A. K. Ghosh, B. Schwarz, M. Strongin, P. B. Allen, and J. W. Halley, Phys. Rev. Lett. **38**, 782 (1977).
[26]B. Chakraborty and P. B. Allen, Phys. Rev. Lett. **42**, 736 (1979).
[27]Charles Kittel, *Introduction to Solid State Physics*, 7th ed. (Wiley Student Edition, Reprint 2006), Chap. 6.
[28]P. C. Canfield, J. D. Thompson, W. P. Beyermann, A. Lacerda, M. F. Hundley, E. Peterson, Z. Fisk, and H. R. Ott, J. Appl. Phys. **70**, 5800 (1991).
[29]M. Bouvier, P. Lethuillier, and D. Schmitt, Phys. Rev. B **43**, 13137 (1991).
[30]S. Ramakrishnan, N. G. Patil, Aravind D. Chinchure, and V. R. Marathe, Phys. Rev. B **64**, 064514 (2001).
[31]V. R. Marathe and S. Mitra, J. Chem. Phys. **78**, 915 (1983).
[32]C. Cascales, P. Porcher, and R. Saez-Puche, J. Phys. Chem. Solids **54**, 1471 (1993).
[33]N. G. Patil and S. Ramakrishnan, Phys. Rev. B **56**, 6 (1997).
[34]T. Moriya and T. Takimoto, J. Phys. Soc. Jpn. **8**, 960 (1995).
[35]G. G. Lonzarich, in *The Electron*, edited by M. Springford (Cambridge University Press, Cambridge, 1997), Chap. 6.
[36]L. Klein, L. Antognazza, T. M. Geballe, M. R. Beasley, and A. Kapitulnik, Phys. B (Amsterdam) **261**, 431 (1999).
[37]R. J. Birgeneau, M. T. Hutchings, J. M. Baker, and J. D. Riley, J. Appl. Phys. **40**, 1070 (1969).
[38]D. C. Mattis, *Theory of Magnetism* (Harper & Row, New York, 1965).
[39]P. G. de Gennes, J. Phys. Radium **23**, 510 (1962).
[40]D. R. Noakes and G. K. Shenoy, Phys. Lett. A **91**, 35 (1982).